Available online at www.jourcc.com

Journal homepage: www.JOURCC.com

Journal of Composites and Compounds

A numerical model for investigation of dynamic behavior and free vibration of functionally graded cylindrical helical springs

Zohreh Ebrahimi [a]*, *Masoud Abasi Atibeh* [a]

[a] *Department of Mechanical Engineering, Payame Noor University, Tehran, Iran*

ABSTRACT

The aim of this paper is to investigate the free vibration of functional-graded (FG) cylindrical helical springs. Model differential equations of homogeneous helical springs are extended to the vibration of FG helical springs. The equations are discretized using finite difference method for space. The time dependent equations are solved using a GMRES method. The initial axial and rotational displacements are applied at the free end of the spring manually and then released. The validated numerical model is then adopted to establish the effects of the FG material index on the model natural frequencies obtained by FFT analysis. According to the results, in both homogeneous and FG helical springs, the amplitudes of axial and rotational displacements increase as they approach the free end of the spring. The numerical results indicate that the FG material index strongly affects the dynamic behavior of the cylindrical helical springs. The amplitudes of the oscillations are damped efficiently and by increasing the material gradient index. ©2021 JCC Research Group.

Peer review under responsibility of JCC Research Group

ARTICLE INFORMATION

Article history:

Received 4 July 2021

Received in revised form 3 August 2021

Accepted 29 August 2021

Keywords:

FG material

Helical spring

Axial and rotational displacement

Gradient index

1. Introduction

Helical springs are widely used in engineering applications. The numerical modeling of the helical springs is of particular importance, due to their nonlinear and complex behavior. The helical spring exhibits a coupled extensional-rotational deformation and is a nonlinear mechanical element [1]. A wide variety of complex vibration problems of the helical springs are reported in the literature. Banerjee et al. [2] solved the free vibration analysis of helical springs to obtain the dynamic stiffness of these springs. Lee et al. [3] investigated the governing equations of helical cylindrical springs based on the Timoshenko beam theory in a curvilinear coordinate system. Temel et al. [4] investigated the forced vibration of helical cylindrical rods under impulsive loads in the frequency domain. Using the continuity approach, Howson et al. [5] obtained natural frequencies for the coupled tensile-rotational movement of the springs and the coupled deformation of the composite rods. Leamy [6] investigated the forced vibrations of helical springs using the finite element method. Champion et al. [7] modeled deviations from the linear spring model for vertically suspended springs. Michalczyk [8] has investigated the effect of using damping coatings on the spring, its vibration, and resonance. He showed that if the entire surface of the spring were covered with the above coatings, the natural first frequency of the spring would be reduced. Yengejeh et al. [9] have simulated vibration and buckling behavior of the helical carbon nanotubes using a finite element method. Vebil [10] proposed a closed-form formula for a closed and open cylindrical spring using an artificial neural network. Crescenzo et al. [11] investigated the two-dimensional buckling behavior of uniform helical springs using lumped stiffness. Kacar et al. [12] utilized the stiffness matrices to obtain natural frequencies and buckling loads of non-uniform helical springs made of composite materials, based on first-order shear deformation theory. A geometrically exact beam theory is applied to model the dynamics of helical springs by Zhang et al. [13]. In another study, Michalczyk et al. [14] presented a simple formula for calculating the natural frequency of transverse vibrations of axial steel helical springs using a modified equivalent Timoshenko beam theory. They have determined a critical axial force, when the first natural frequency becomes zero.

FG materials exhibit different properties in different regions of the material due to the gradual change of chemical composition, distribution, and orientation or size of the constituent phases in one or more dimensions. This gradual change of the structure and properties has led to the extensive use of these materials such as biomedical, aerospace, defense, energy, automobiles, marine, constructions, and so on [15]. The nonlinear vibration problems of complete and incomplete FG cylindrical shells with elastic bases have been studied in the literature using the classical shell theory and with Galerkin and harmonic equilibrium superposition [16, 17]. Dung et al. [18] solved the post-buckling problem of reinforced FG cylindrical shells under axial-compressive loads and on elastic foundations using the classical shell theory. Anh et al. [19] studied the nonlinear vibration and dynamic response of stiffened FG cylindrical shells on elastic foundations in thermal environments. Recently, Liu et al. presented a numerical model to predict compressive behavior of composite helical springs [20]. They have obtained more accurate results by including geometrical nonlinearity into their model.

* *Corresponding author: Zohreh Ebrahimi; E-mail: z.ebrahimi@pnu.ac.ir*

DOR: 20.1001.1.26765837.2021.3.8.5.2

https://doi.org/10.52547/jcc.3.3.5

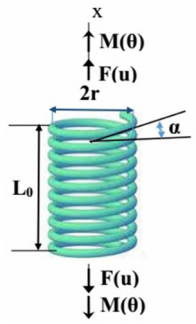

Fig. 1. Schematic of a cylindrical helical spring with applied force and moment.

Helical springs are important mechanical elements due to their widespread use [21]. From the above discussed literature, it is established that FG materials have removed considerable restrictions in many industries. Therefore, the FG helical springs can be used efficiently in engineering applications. On the other hand, aluminum based metal FG materials are very popular due to their high strength to weight ratio and good resistance [22]. A common non-metallic reinforcement phase embedded in this composite is silicon carbide (SiC) [23]. The presented research investigates the dynamics response and free vibration of the Al-SiC functionally graded helical springs using a coupled axial-torsional model. The coupled axial-torsional vibration of a homogeneous helical spring is first proposed by Jiang et al. [1]. This model is extended to free vibration of the Al-SiC functionally graded helical spring in this paper. The dynamic behavior and the time histories of the axial and rotational displacements are evaluated. The equations are discretized using finite difference method for space and the time dependent equations are solved using a GMRES method [24].

According to the authors knowledge, no work has been reported on free vibration analysis of the FG helical springs. In most of the mentioned literature, the dynamic response of the homogeneous helical spring is established. Therefore, this paper aims to address the dynamic behavior and free vibration of the FG helical springs as truly as possible.

2. Materials and Methods

2.1 Helical spring equations of motion

If no distributed load is applied on the helical spring, it can be deformed to another helical spring under the axial force F and the torsional moment M. This exerts equal torsion at both ends of the spring [1]. Figure 1 shows the helical spring under force and moment. In this case, the non-zero internal moment and forces are constant along the centerline of the spring.

The force-strain relation is expressed as Eq. (1),

$$M = k_3\varepsilon + k_4\varphi \quad F = k_1\varepsilon + k_2\varphi \tag{1}$$

In the above relations, ε and φ are axial and rotational strains, respectively. According to Ref. [1], the stiffness constants of the spring can be written as Eq. (2),

$$\begin{aligned} k_1 &= \frac{\pi E R^4}{r^2\Delta}(1+k^2(1+\nu)), k_2 = \frac{\pi\nu E R^4 k}{r\Delta} \\ k_3 &= -\frac{\pi E R^4 k}{4r\Delta}(4\nu+\frac{R^2}{r^2}), \\ k_4 &= \frac{\pi E R^4}{4\Delta}(4(1+\nu+k^2)+\frac{k^2R^2}{r^2}) \end{aligned} \tag{2}$$

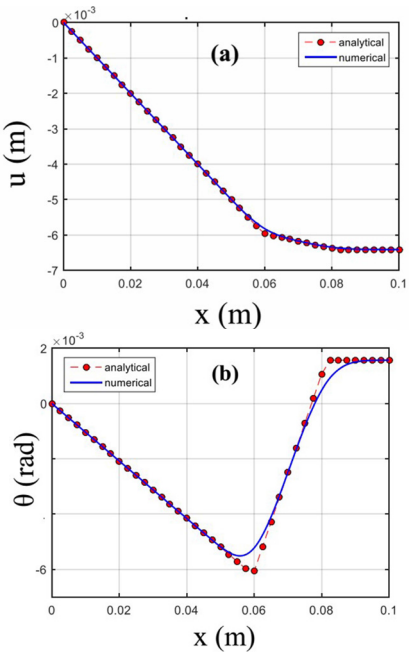

Fig. 2. Analytical and numerical axial displacement (a) and rotational displacement (b) versus position along homogeneous spring length at t=0.001.

where r is the radius of the spring coil, R is radius of the spring wire, k is the tangent of helical angle, E is the elasticity module, and υ is the poison's ratio. The parameter Δ is given in Eq. (3),

$$\Delta = \frac{1}{k\sqrt{1+k^2}}\left(4(1+\nu)(1+k^2)^2 + \frac{k^2R^2}{r^2}((1-\nu)+k^2(1+\nu))\right) \tag{3}$$

According to linear force-strain relations (Eq. 1 and Eq. 2), the governing equations for small displacements of the spring are obtained as Eq. (4),

$$\begin{aligned} k_1\frac{\partial^2 u}{\partial x^2} + k_2\frac{\partial^2\theta}{\partial x^2} &= \gamma\frac{\partial^2 u}{\partial t^2} \\ k_3\frac{\partial^2 u}{\partial x^2} + k_4\frac{\partial^2\theta}{\partial x^2} &= \mu\frac{\partial^2\theta}{\partial t^2} \end{aligned} \tag{4}$$

where $u(x,t)$ is the axial displacement, $\theta(x,t)$ is the rotational displacement of the spring, γ is the mass per unit length and μ is the mass moment of inertia per unit length of the spring.

2.2 Helical spring free vibrations

To investigate the free vibration of the cylindrical helical spring, one end of the spring is considered to be fixed at x=0, and the other end is free at x=L_0. L_0 is the free length of the spring. The initial displacement and rotation, u_0 and θ_0, are applied at the free end of the spring. These initial displacements are dropped suddenly at the beginning of the motion at t=0, and the helical spring vibrates freely. The initial and boundary conditions of the problem are given in Eq. (5),

$$\begin{aligned} &u(x,0) = \frac{u_0}{L_0}x, \theta(x,0) = \frac{\theta_0}{L_0}x \\ &\frac{\partial}{\partial t}u(x,0) = 0, \frac{\partial}{\partial t}\theta(x,0) = 0 \\ &u(0,t) = 0, \theta(0,t) = 0, \\ &\frac{\partial}{\partial x}u(L_0,t) = 0, \frac{\partial}{\partial x}\theta(L_0,t) = 0, \end{aligned} \tag{5}$$

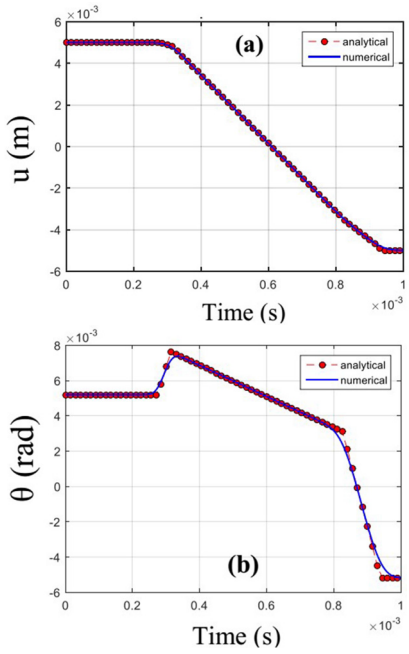

Fig. 3. Analytical and numerical axial displacement (a) and rotation (b) versus time at x=L/2.

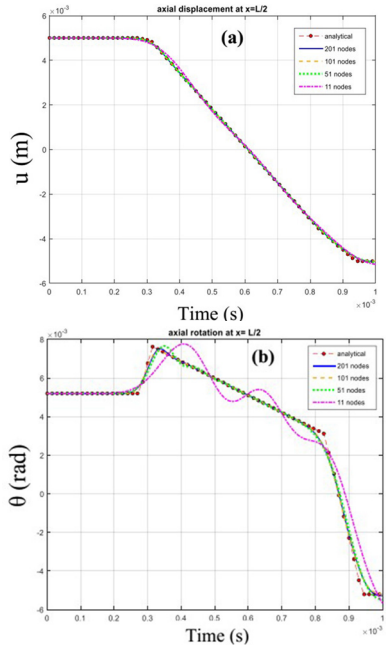

Fig. 4. Axial displacement (a) and rotational displacement (b) at x=L/2 for different number of nodes.

Regarding the coupled behavior of the cylindrical helical springs, the relationship $\theta_0 = -k_3 / k_2 u_0$ exists between the initial displacements. The discretization of the system governing equations is the first step of solving them. Since the equations are second order in time, three consecutive time steps are required. Eq. (4) is rewritten in Eq. (6) by defining $\frac{\partial u}{\partial t} = P$, and $\frac{\partial \theta}{\partial t} = S$,

$$k_1 \frac{\partial^2 u}{\partial x^2} + k_2 \frac{\partial^2 \theta}{\partial x^2} = \gamma \frac{\partial P}{\partial t}$$
$$k_3 \frac{\partial^2 u}{\partial x^2} + k_4 \frac{\partial^2 \theta}{\partial x^2} = \mu \frac{\partial S}{\partial t} \qquad (6)$$

The resulting equations are first order in time. A central difference scheme is used for spatial discretization. The computational domain is one-dimensional with IN nodes along the spring helix centerline. For solving the discretized system of equations, a GMRES method [24] is used in each time step.

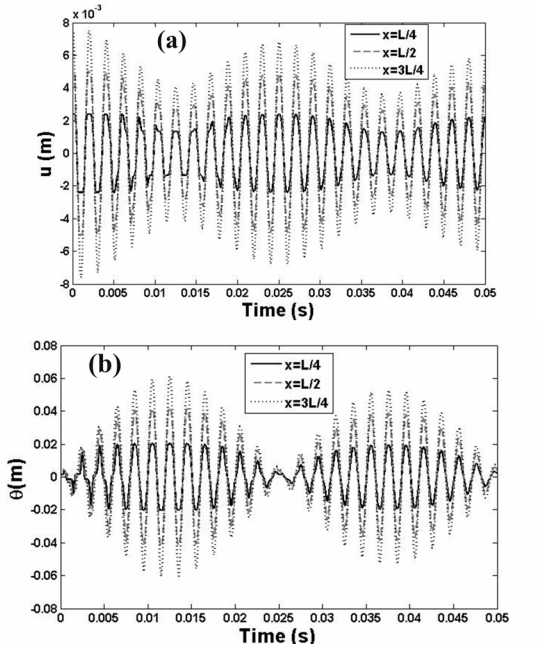

Fig. 5. Time histories of axial (a) and rotational (b) displacements at x=L/4, L/2 and, 3L/4 for homogeneous helical spring.

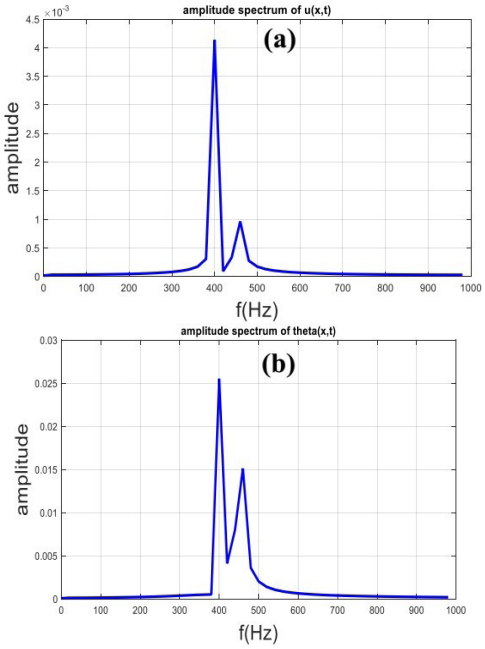

Fig. 6. FFT diagram of oscillation amplitude versus frequency for axial displacement (a) and rotation (b) of a homogeneous helical steel.

In this study, the cylindrical helical FG spring is composed of the silicon-carbide ceramic and aluminum (Al-SiC). The spring module of elasticity, density and poison's ratio varies gradually along the spring centerline. The mechanical properties in each point are defined using a power law function as related in Eq. (7).

$$E(x) = E_{Al} + (E_{SiC} - E_{Al})\left(\frac{L_0 - L(x)\bar{L}_0}{L_0}\right)^n,$$
$$\rho(x) = \rho_{Al} + (\rho_{SiC} - \rho_{Al})\left(\frac{L_0 - L(x)\bar{L}_0}{L_0}\right)^n, \qquad (7)$$
$$\nu(x) = \nu_{Al} + (\nu_{SiC} - \nu_{Al})\left(\frac{L_0 - L(x)\bar{L}_0}{L_0}\right)^n$$

where n is the gradient index and $\bar{L}_0 = L_0 / 2\pi R N_t$. L(x) is the

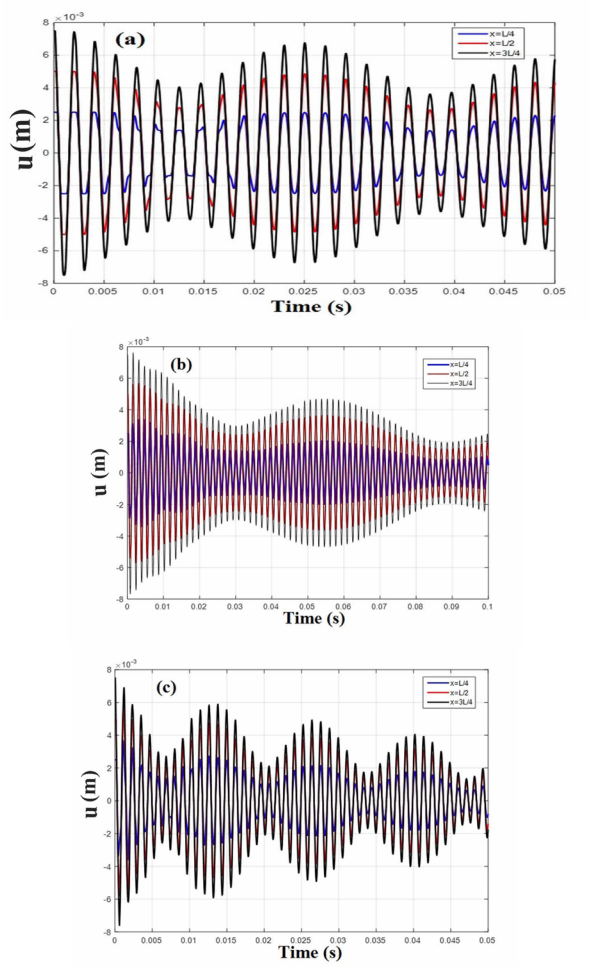

Fig. 7. Time histories of axial displacement at x=L/4, L/2 and, 3L/4 for the FG helical spring with n=0 (a), n=0.25 (b) and n=0.5 (c).

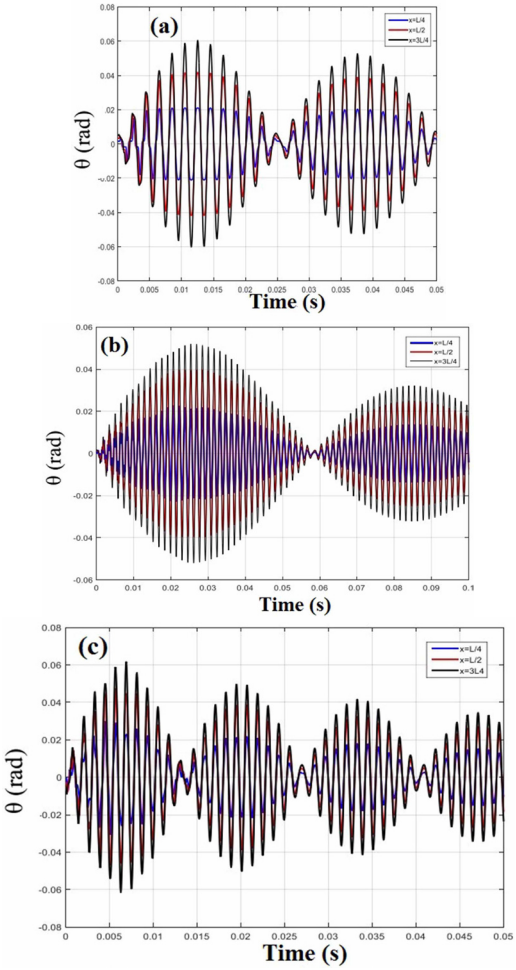

Fig. 8. Time histories of rotational displacement at x=L/4, L/2 and, 3L/4 for the FG helical spring with n=0 (a), n=0.25 (b) and n=0.5 (c).

spring length, which can be written as, $L(x) = 2\pi RN_t x / L_0$. The total number of spring coils is presented with N_t.

3. Results and Discussions

3.1 Homogeneous helical spring Model

First, the numerical results are compared with the analytical formula of Ref. [1] to verify the numerical procedure. Therefore, a cylindrical helical spring made of steel with E=200 GPa, ν=0.29, and ρ= 7600 (kg/m3) is considered for model validation. The geometrical parameters are R=0.01 m, r=0.1 m, α=π/6, where α is the spring helical angle. The spring free length and the number of spring coils are L_0=0.2 m and N_t=6, respectively. The initial axial and rotational displacements applied at the free end of the spring, are u_0=0.01 m and θ_0=-(k_3/k_2)u_0, respectively. The initial displacements are dropped suddenly at t=0 and the spring begins to vibrate.

The analytical formula for the axial-torsional coupled motion of the helical springs proposed by Jiang et al. [1] are implemented in a Matlab code and the results are compared with those of the presented numerical model. As stated before, in the presented numerical model the time dependent discretized model equations are solved using GMRES method. The analytical and numerical axial and rotational displacements versus position are shown in Figure 2 and Figure 3, for homogeneous spring at t=0.001 s. An excellent agreement is obtained between numerical and analytical results.

A grid study is performed to find an optimized number of computational nodes. The results are illustrated in Figure 4. The axial and rotational displacements are plotted at the middle of the spring for k=11, 51, 101, and 201, where k is the number of nodes in the computational domain. As it can be seen, by using a finer grid, i.e., increasing the number of nodes, the results converge to the analytical values. The convergence is obtained for k≥51. Therefore an optimum value of k=51 is used for further simulations.

The fixed end of the spring is placed at x=0. Therefore, the amplitudes of axial and rotational oscillations will increase as x approaches to the free end of the spring. However, to establish the increasing of these amplitudes more accurately, the temporal evolutions of the axial displacements at x=L/4, L/2, and 3L/4 are presented in Figure 5 (a). Time histories of rotational displacements at the same positions are also presented in Figure 5 (b). As shown in Figure 5 (a), the axial displacement of the spring versus time is periodic with sine waves. The amplitudes of the oscillations at x=L/4, L/2, and 3L/4 are different, but the general behavior of these oscillations is the same. Moreover, the amplitudes of the oscillations become larger by approaching the free end of the spring. The amplitude of the oscillation at x=3L/4 is greater than x= L/4 and L/2.

According to Figure 5 (b), the general behavior of rotational displacement oscillations is the same for all three positions. The number and period of cycles in a given time interval are the same as well. However, the amplitudes of the rotational displacement oscillations are different at these three points. The closer one gets to the free end of the spring, the more the rotational displacement increases.

Main frequencies of the homogeneous helical spring are obtained by Fast Fourier Transformation (FFT). The FFT is often utilized to identify the nonlinear structural elements in frequency domain analysis [25]. The

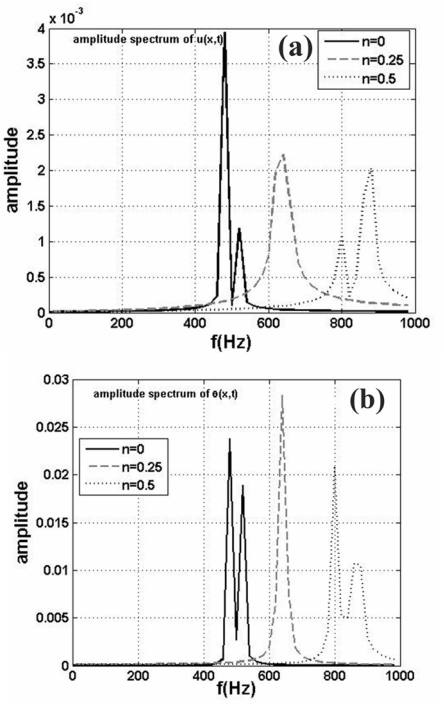

Fig. 9. FFT diagram of oscillation amplitude versus frequency for axial displacement (a) and rotational displacement (b) of the FG helical spring.

oscillation amplitudes for FFT of axial displacement and rotation versus their motion frequencies are shown in Figure 6 (a) and 6 (b), respectively. Two maximum frequencies are observed in these figures, which are the first and second main frequencies. For the axial displacement, the main frequencies are 460 and 400 Hz. The related amplitude of these oscillations are 0.0041 and 0.001 m, respectively. For the rotational displacement, the main frequencies are 460 and 400 Hz with amplitudes of 0.0255 and 0.0151 m.

3.2 FG helical spring Model

Next, the FG cylindrical helical spring model is considered. Table 1 presents the mechanical properties of the FG material. The fixed end of the spring is SiC ceramic, and the free end of the spring is aluminum. The mechanical properties change gradually along the spring length, L(x). Geometrical parameters are the same as the previous simulation.

The initial displacements u_0=0.01 m and θ_0=-(k_3/k_2)$u_{0,}$ are removed suddenly at t=0 and the spring free vibration starts. Since E, ν, and ρ are functions of x, the spring coefficients k_3 and k_4 are position-dependent, as well. Therefore, θ_0 is not constant. The discretized equations are evaluated in each computational node. The time step of 10^{-6} is used. The system of discretized equations is solved by applying the GMRES method in MATLAB programming software. The effects of the gradient index of FG material on free vibration of the FG helical spring are studied.

Three gradient index values n =0, n=0.25, and n=0.5 are considered. As related in Eq. 1 to Eq. 3, the zero gradient index results in a homogeneous helical spring. Figure 7 shows the time histories of axial displacement of the FG spring at x=L/4, L/2, and 3L/4. The shape of axial displacement is different for three values of the gradient index. The oscillation period and amplitude are not the same for different values of the gradient index. For the FG helical spring with n=0.25 and n=0.5, as shown in Figure 7 (b) and (c), the amplitudes decrease as time evolves and, the vibration is damped after passing some time. However, the amplitudes remain constant for n=0.0 within the same time interval as illustrated in Figure 7 (a). The oscillation period for n=0.25 is greater than that of n=0 and n=0.5. Therefore, the time interval for this simulation is 0.1 s to illustrate the dynamic behavior and decreasing trend of the oscillation amplitudes for n=0.25, more accurately.

Table 1.
Mechanical properties of the FG material

Property	Value
E_{Al} (Pa)	70×10^9
ν_{Al}	0.3
ρ_{Al} (kg/m^3)	2702
E_{SiC} (Pa)	427×10^9
ν_{SiC}	0.17
ρ_{SiC} (kg/m^3)	3100

The rotational displacement of the FG helical spring is presented in Figure 8. For n=0, the material is homogeneous. By increasing the gradient index, the oscillation behavior of the rotational displacements changes. The maximum value of these oscillations is constant for n=0 and decreases gradually for n=0.25 and n=0.5. The variation of the oscillation period is observed for the rotational displacements as well. The oscillation period has the biggest value for n=0.25, hence the time interval is set to 0.1 s for this simulation.

Decreasing of the oscillation amplitudes is observed only for the FG helical springs. Following the trends of the oscillation amplitudes for n=0.5, complete damping of the oscillation will occur after 0.15 s. For n=0.25, the time required for complete damping of the oscillations is 0.25 s.

The main frequencies of the FG helical spring and their related oscillation amplitudes versus gradient index are evaluated by FFT analysis. The oscillation amplitudes for FFT of the axial and rotational displacements versus their motion frequencies are shown in Figures 9 (a) and 9 (b), respectively. For each FFT analysis, two maximum frequencies are observed, which are the first and second main frequencies. The main frequency values and their related amplitudes are summarized in Table 2 for three gradient index values, i.e., n=0, 0.25, 0.5.

The results of Table 2 show that the main frequencies of the free vibration of the FG helical spring are increased with increasing the gradient index from 0 to 0.5. According to the presented results, the amplitude of axial and rotational displacements of the FG helical spring with n = 0.25 are less than those of homogeneous helical spring, which have been reported by Jiang et al [1]. The rotational displacement amplitudes of the FG helical spring with n=0.5 are less than those of the homogeneous helical spring. On the other hand, the rotational displacement amplitude corresponding to the first and second frequencies of the FG helical spring with n=0.5 is greater than the rotational displacement amplitude corresponding to the first frequency and less than the rotational amplitude corresponding to the second frequency of the FG helical spring with n=0.25. The axial displacement amplitude corresponding to the first frequency of the FG helical spring with n=0.5 is less than those of the homogeneous spring and those of the FG spring with n=0.25. However, the amplitudes of the displacement corresponding to the second frequency for the FG helical spring with n=0.5 are more significant than those of the homogeneous helical spring and those of the FG helical spring with n=0.25.

4. Conclusion

In this study, the free vibration of a functionally graded cylindrical helical spring has been investigated. The analytical formula for the axial-torsional coupled motion of the helical spring proposed by Jiang et al. [1] has been used for model validation. An excellent agreement has been obtained between numerical and analytical results, which indicates the high efficiency of the presented numerical model. The effects of the FG material index on dynamic behavior of the Al-SiC functionally graded helical spring have been investigated.

Table 2.
Main frequencies and amplitudes for the vibration of the FG helical spring with different gradient index values

	n=0.0		n=0.25		n=0.5	
	First frequency (Hz)	Second frequency (Hz)	First frequency (Hz)	Second frequency (Hz)	First frequency (Hz)	Second frequency (Hz)
	480	520	630	650	800	880
Axial displacement amplitude (m)	0.0039	0.0012	0.0028	0.0009	0.0011	0.0020
Rotational displacement amplitude (rad)	0.0238	0.0189	0.0160	0.0171	0.0209	0.0108

The numerical results of the presented model indicate that FG material index strongly affects the dynamic behavior of the cylindrical helical springs. The oscillation period, oscillation amplitudes and model natural frequencies have been changed by gradient index variation. With increasing the gradient index, the vibrational oscillations were damped faster. This study has discovered that the application of FG materials in design of helical springs increases the damping capacity and vibration resistance of these structures. The proposed numerical model can be extended to non-cylindrical springs and has provided insights into the optimal design of helical structures in engineering applications.

Acknowledgments

The authors would like to acknowledge Payame Noor University for the financial support towards this research.

Conflict of interest

The authors declare that there is no conflict of interest.

REFERENCES

[1] W. Jiang, W. Jones, T. Wang, and K. Wu, Free vibration of helical springs, Journal of Applied Mechanics 58(1) (1991) 222-228.
[2] J. Banerjee and F. Williams, An exact dynamic stiffness matrix for coupled extensional-torsional vibration of structural members, Computers & structures 50(2) (1994) 161-166.
[3] J. Lee and D. Thompson, Dynamic stiffness formulation, free vibration and wave motion of helical springs, Journal of Sound and Vibration 239(2) (2001) 297-320.
[4] B. Temel and F. F¸ Calim, Forced vibration of cylindrical helical rods subjected to impulsive loads, Journal of Applied Mechanics 70(2) (2003) 281-291.
[5] W. P. Howson and B. Rafezy, Natural frequencies of axial–torsional coupled motion in springs and composite bars, Journal of sound and vibration 330(15) (2011) 3636-3644.
[6] M. J. Leamy, Intrinsic finite element modeling of nonlinear dynamic response in helical springs, Journal of computational and nonlinear dynamics 7(3) (2012) 031007.
[7] R. Champion and W. Champion, Departure from linear mechanical behavior of a helical spring, Mathematical and Computer Modelling 53(5) (2011) 915-926.
[8] K. Michalczyk, Dynamic stresses in helical springs locally coated with highly-damping material in resonant longitudinal vibration conditions, International Journal of Mechanical Sciences 90 (2015) 53-60.
[9] S. I. Yengejeh, S. A. Kazemi, and A. Öchsner, On the buckling and vibrational response of carbon nanotubes with spiral deformation, Journal of Theoretical and Applied Mechanics 54(2) (2016) 613-619.
[10] Y. Vebil, A Closed-Form Buckling Formula for Open-Coiled and Properly Supported Circular-Bar Helical Springs, Strojnícky časopis-Journal of Mechanical Engineering 68(3) (2018) 33-48.
[11] F. De Crescenzo and P. Salvini, Two-Dimensional Discrete Model for Buckling of Helical Springs, Procedia Structural Integrity 24 (2019) 28-39.
[12] I. Kacar and V. Yildirim, Free vibration/buckling analyses of noncylindrical initially compressed helical composite springs, Mechanics Based Design of Structures and Machines 44(4) (2016) 340-353.
[13] J. Zhang, Z. Qi, G. Wang, and S. Guo, High-efficiency dynamic modeling of a helical spring element based on the geometrically exact beam theory, Shock and Vibration 2020 (2020) 8254606.
[14] K. Michalczyk, P. Bera, A Simple formula for predicting the first natural frequency of transverse vibrations of axially loaded helical springs, Journal of Theoretical and Applied Mechanics 57(3) (2019) 779-790.
[15] P. M. Pandey, S. Rathee, M. Srivastava, P. K. Jain, Functionally Graded Materials (FGMs): Fabrication, Properties, Applications, and Advancements, first ed., CRC Press, USA, 2022.
[16] M. Mehri, H. Asadi, and Q. Wang, Buckling and vibration analysis of a pressurized CNT reinforced functionally graded truncated conical shell under an axial compression using HDQ method, Computer Methods in Applied Mechanics and Engineering 303 (2016) 75-100.
[17] A. Najafov, A. Sofiyev, The non-linear dynamics of FGM truncated conical shells surrounded by an elastic medium, International Journal of Mechanical Sciences 66 (2013) 33-44.
[18] D. Van Dung, B. T. T. Hoai, Postbuckling nonlinear analysis of FGM truncated conical shells reinforced by orthogonal stiffeners resting on elastic foundations, Acta Mechanica 228(4) (2017) 1457-1479.
[19] V. T. T. Anh, N. D. Duc, Vibration and nonlinear dynamic response of eccentrically stiffened functionally graded composite truncated conical shells surrounded by an elastic medium in thermal environments, Acta Mechanica 230(1) (2019) 157-178.
[20] L. Wu, L. Chen, H. Fu, Q. Jiang, X. Wu, Y. Tang, Carbon fiber composite multistrand helical springs with adjustable spring constant: design and mechanism studies, Journal of Materials Research and Technology 9(3) (2020) 5067-5076.
[21] T.W. Liu, J.B. Bai, Q.H. Lin, Q. Cong, An analytical model for predicting compressive behaviour of composite helical Structures: Considering geometric nonlinearity effect, Composite Structures 255 (2021) 112908.
[22] I.M. El-Galy, M.H. Ahmed, B.I. Bassiouny, Characterization of functionally graded Al-SiCp metal matrix composites manufactured by centrifugal casting, Alexandria Engineering Journal 56(4) (2017) 371–381.
[23] M.S. Surya, G. Prasanthi, Tribological Behaviour of Aluminum Silicon Carbide Functionally Graded Material 40 (2) (2018) 247-253.
[24] Y. Saad, M.H. Schultz, GMRES: A generalized minimal residual algorithm for solving nonsymmetric linear systems, SIAM Journal on scientific and statistical computing 7(3) (1986) 856-869.
[25] A. Alizadeh, Z. Ebrahimi, A. Mazidi, S. Ahmad Fazelzadeh, Experimental Nonlinear Flutter Analysis of a Cantilever Wing/Store, International Journal of Structural Stability and Dynamics 20 (7) (2020) 2050082.